

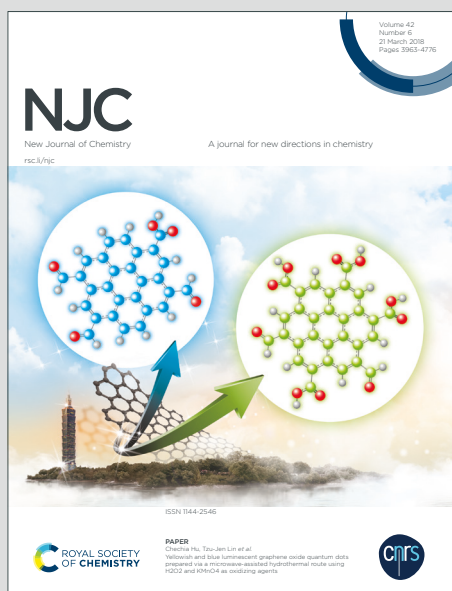
# NJC

New Journal of Chemistry

Accepted Manuscript

A journal for new directions in chemistry

This article can be cited before page numbers have been issued, to do this please use: R. Jahanshahi, A. Khazaei, S. Sobhani and J. Sansano, *New J. Chem.*, 2020, DOI: 10.1039/D0NJ01599G.



This is an Accepted Manuscript, which has been through the Royal Society of Chemistry peer review process and has been accepted for publication.

Accepted Manuscripts are published online shortly after acceptance, before technical editing, formatting and proof reading. Using this free service, authors can make their results available to the community, in citable form, before we publish the edited article. We will replace this Accepted Manuscript with the edited and formatted Advance Article as soon as it is available.

You can find more information about Accepted Manuscripts in the [Information for Authors](#).

Please note that technical editing may introduce minor changes to the text and/or graphics, which may alter content. The journal's standard [Terms & Conditions](#) and the [Ethical guidelines](#) still apply. In no event shall the Royal Society of Chemistry be held responsible for any errors or omissions in this Accepted Manuscript or any consequences arising from the use of any information it contains.

# g-C<sub>3</sub>N<sub>4</sub>/γ-Fe<sub>2</sub>O<sub>3</sub>/TiO<sub>2</sub>/Pd: A new magnetically separable photocatalyst for visible-light-driven fluoride-free Hiyama and Suzuki–Miyaura cross-coupling reactions at room temperature

View Article Online

DOI: 10.1039/x0xx00000x

Received 00th January 20xx,  
Accepted 00th January 20xx

DOI: 10.1039/x0xx00000x

Roya Jahanshahi,<sup>a</sup> Asma Khazaei,<sup>a</sup> Sara Sobhani\*<sup>a</sup> and José Miguel Sansano<sup>b</sup>

In this paper, a new visible-light harvesting photocatalyst denoted as g-C<sub>3</sub>N<sub>4</sub>/γ-Fe<sub>2</sub>O<sub>3</sub>/TiO<sub>2</sub>/Pd was successfully fabricated and fully characterized by different techniques including FT-IR, XPS, XRD, TEM, SEM, elemental mapping, VSM, DRS, and ICP analysis. The as-prepared catalyst was utilized as an efficient magnetically separable photocatalyst in the fluoride-free Hiyama and Suzuki–Miyaura cross-coupling reactions at room temperature under visible light irradiation. By using this approach good to excellent yields of biaryls were achieved from the reaction of various aryl iodides/bromides and even chlorides as the highly challenging substrates, which are more available and cheaper than aryl iodides and bromides, with triethoxyphenylsilane or phenylboronic acid. The superior photocatalytic activity of g-C<sub>3</sub>N<sub>4</sub>/γ-Fe<sub>2</sub>O<sub>3</sub>/TiO<sub>2</sub>/Pd could be attributed to the synergistic catalytic effects of Pd nanoparticles and g-C<sub>3</sub>N<sub>4</sub>/γ-Fe<sub>2</sub>O<sub>3</sub>/TiO<sub>2</sub>. Utilizing the sustainable and safe light source, no need to use any additive or heat, using an eco-friendly solvent and long-term stability and magnetic recyclability of the catalyst for at least seven successive runs are the advantages that support the current protocol towards the green chemistry.

## Introduction

In the past few decades, novel approaches have focused on the development of more environmentally compatible chemical processes in both academic and industrial viewpoints. The major criteria that support a chemical transformation towards green chemistry are utilizing the environmentally benign energy sources and solvents, and avoiding waste formation by using the separable heterogeneous catalysts.<sup>1</sup>

As an ideal renewable energy source, solar energy intended to be the most promising choice for conducting eco-friendly photocatalytic processes.<sup>2</sup> Considering that a great portion of sunlight (44%) devotes to the visible area, the development of visible-light harvesting photocatalytic systems to drive chemical processes has attracted a growing interest with every passing year.<sup>3</sup> TiO<sub>2</sub> is one of the most favorable semiconductor candidates in the photocatalysis area due to its outstanding properties including chemical and physical durability, photo-corrosion resistance, low toxicity, and cost-effectiveness.<sup>4,5</sup> However, the main challenging aspect with using TiO<sub>2</sub> is its broad band gap (E<sub>g</sub> = 3.2 eV) that limits its photocatalytic performance only to the UV-light area (3-5% of total solar energy).<sup>6</sup> Furthermore, the photo-generated electron-hole pairs in TiO<sub>2</sub> can be readily recombined, which critically diminished its optical efficiency.<sup>7</sup> One of the most efficient proposed approaches to amend the visible-light photocatalytic properties of TiO<sub>2</sub> is its combination with other semiconductors to prepare composite

photocatalysts.<sup>8</sup> Recently, graphitic carbon nitride (g-C<sub>3</sub>N<sub>4</sub>), a polymeric metal-free material has been extensively investigated as a semiconductor photocatalyst.<sup>9</sup> Although it has benefits of ease of preparation, excellent visible-light harvesting ability (band gap = 2.73 eV), nontoxicity, low-cost and high thermal/chemical stability, the low separation efficiency and prompt recombination rate of the photo-generated electrons and holes, significantly confine its photocatalytic performance.<sup>10-12</sup> Fascinatingly, the semiconductor combination of g-C<sub>3</sub>N<sub>4</sub> with TiO<sub>2</sub> cannot only overcome the elevated recombination speed of the resultant photo-excited electron and hole pairs of both semiconductors but also enhances the visible light absorption potential of TiO<sub>2</sub>.<sup>13</sup>

Cross-coupling reactions catalyzed by transition metals are the most popular, straightforward, and powerful protocols for the preparation of carbon-carbon bonds in organic chemistry. Among these, Hiyama and Suzuki–Miyaura cross-coupling reactions have attracted a great deal of attention for the efficient and direct synthesis of biaryls from the reactions of aryl halides and organosilicon/organoboron reagents.<sup>14,15</sup> The resulting coupling products are widely applied as basic building blocks for the fabrication of diverse molecules in several fields of chemistry such as material sciences, pharmacy, and agrochemistry.<sup>16</sup> From the environmental and economical points of view, organosilicon compounds are the best alternative rather than the other organometallic reagents such as organozinc, organomagnesium, and organotin compounds, owing to their cost-effectiveness, low toxicity, high stability, and wide availability.<sup>17</sup> They are also preferable to organoboron compounds, which are either unstable or difficult to purify and frequently lose boron to give undesirable homo-coupling products. However, the weak polarization of the carbon-silicon bond in organosilicon derivatives makes these reagents to be known as poor cross-coupling partners. Using the fluoride anions as the most common activators can properly promote the nucleophilicity of these organosilicon reagents.<sup>18,19</sup> Nonetheless, the fluoride ion is a strong base and

<sup>a</sup> Address: Department of Chemistry, College of Sciences, University of Birjand, Birjand, Iran, email: ssobhani@birjand.ac.ir, sobhanisara@yahoo.com.

<sup>b</sup> Departamento de Química Orgánica, Facultad de Ciencias, Centro de Innovación en Química Avanzada (ORFEO-CINQA) and Instituto de Síntesis Orgánica (ISO), Universidad de Alicante, Apdo. 99, 03080-Alicante, Spain.

Electronic Supplementary Information (ESI) available: [It contains the spectral data of the products].

## ARTICLE

## Journal Name

therefore functional groups such as base-sensitive protecting groups and acidic protons cannot tolerate the existence of fluoride ions. This limitation has been overcome by the replacement of fluoride ions with inorganic bases.<sup>20-22</sup>

Among the various transition metals developed to catalyze the Hiyama and Suzuki–Miyaura cross-coupling reactions, palladium has been the first choice and is still considered as the most common metal for C–C coupling reactions.<sup>23</sup> Traditionally, these cross-coupling reactions are performed under homogeneous palladium catalytic systems with relatively high activity and selectivity.<sup>24</sup> Nevertheless, these approaches suffer from the separation and recovery limitations encountering by the homogeneous catalysts. The heterogeneous catalysis is advisable for simple product separation and catalyst recycling, which clearly assert the heterogeneous catalytic systems as suitable candidates towards more sustainable and green chemical developments.<sup>25</sup> In this line, extensive efforts have been done to conduct the Hiyama and Suzuki–Miyaura cross-coupling reactions through the heterogeneous Pd-based catalytic systems by Pd immobilization/stabilization on different supports such as mesoporous materials, polymer, graphene oxide, carbon compounds, metal oxides, and magnetic nanoparticles (MNPs).<sup>15,22,26-29</sup> Among these supporting materials, using MNPs has the merit of simple and convenient catalyst isolation from the reaction mixture by using an external magnetic field. The majority of the above-mentioned heterogeneous Pd catalytic systems require elevated temperatures and prolonged reaction times, which may lead to undesired side reactions. Interestingly, coupling reactions can be conveniently performed at room temperature by using light irradiation.<sup>30</sup> However, the reported Pd-based heterogeneous photocatalysts for visible-light-driven Hiyama and Suzuki–Miyaura cross-coupling reactions are limited to a few methods.<sup>31-46</sup> Nevertheless, most of these procedures have witnessed one or more of the following difficulties such as utilizing extra additives, high photocatalyst loading, tedious and time-consuming photocatalyst isolation procedures, photocatalyst loss during the recycling, prolonged reaction times, unsatisfactory yields of the products, and using hazardous solvents, specific atmospheres, and complex photoreactors. Thus, the necessity of promoting a more proficient and eco-benign photocatalytic approach to conduct these transformations through more mild conditions is evident. Moreover, it is worth noting that despite the considerable success achieved in the use of magnetically separable nanocatalysts in organic reactions, the incorporation of magnetic components into the photocatalytic systems to drive the C–C cross-coupling reactions is in the preliminary stages.

Inspired by these facts and as a part of our ongoing efforts regarding the development of new catalytic methods to conduct the cross-coupling reactions through more eco-benign conditions,<sup>47-49</sup> herein, we have successfully synthesized  $g\text{-C}_3\text{N}_4/\gamma\text{-Fe}_2\text{O}_3/\text{TiO}_2/\text{Pd}$  as a new magnetically separable visible-light-driven photocatalyst and characterized it by various techniques. The capability of the photocatalyst was well investigated towards the fluoride-free Hiyama and Suzuki–Miyaura cross-coupling reactions at room temperature under visible light irradiation.

## Results and discussion

Preparation and characterization of  $g\text{-C}_3\text{N}_4/\gamma\text{-Fe}_2\text{O}_3/\text{TiO}_2/\text{Pd}$ 

Figure 1 illustrates the multi-step procedure for the preparation of  $g\text{-C}_3\text{N}_4/\gamma\text{-Fe}_2\text{O}_3/\text{TiO}_2/\text{Pd}$ . At first,  $g\text{-C}_3\text{N}_4/\gamma\text{-Fe}_2\text{O}_3/\text{TiO}_2$  was prepared by a sol-gel procedure from tetrabutyl orthotitanate (TBOT) in the presence of a mixture of separately synthesized  $g\text{-C}_3\text{N}_4$  and  $\gamma\text{-Fe}_2\text{O}_3$ . Next, the reduction of the adsorbed  $\text{Pd}(\text{OAc})_2$  on the surface of  $g\text{-C}_3\text{N}_4/\gamma\text{-Fe}_2\text{O}_3/\text{TiO}_2$  produced  $g\text{-C}_3\text{N}_4/\gamma\text{-Fe}_2\text{O}_3/\text{TiO}_2/\text{Pd}$ .

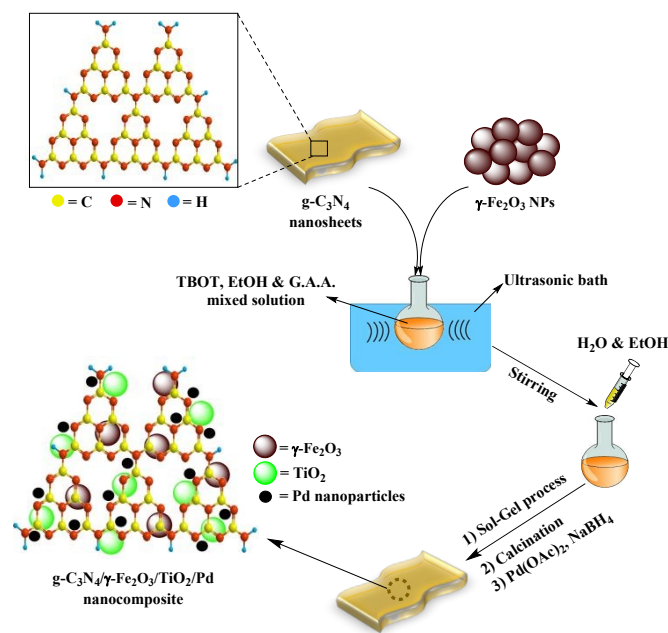
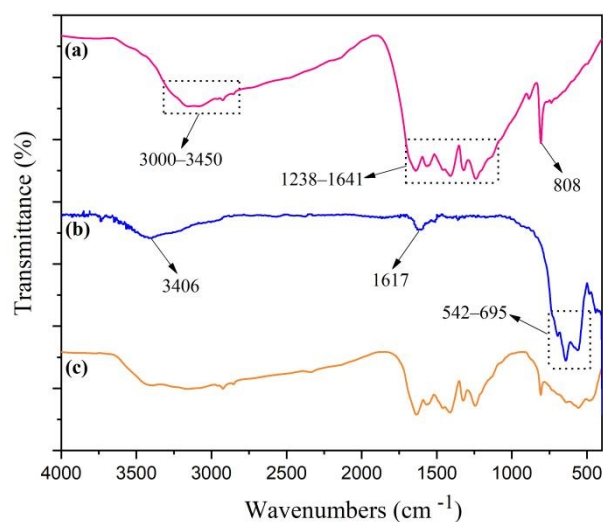


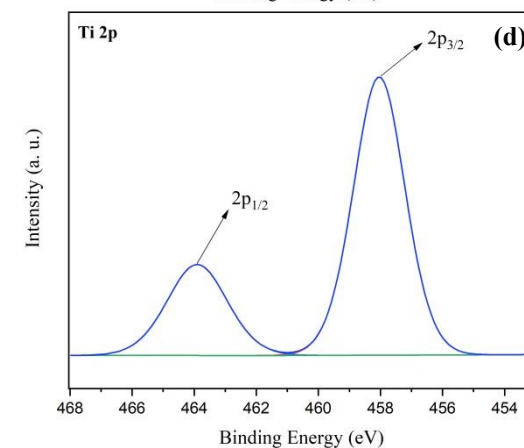
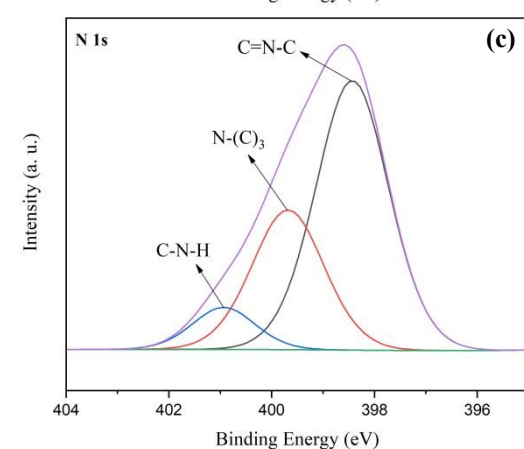
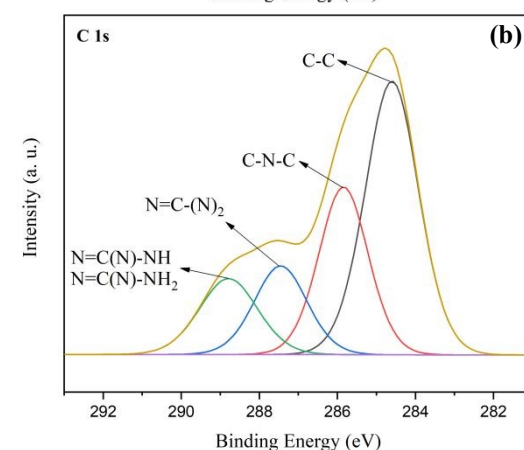
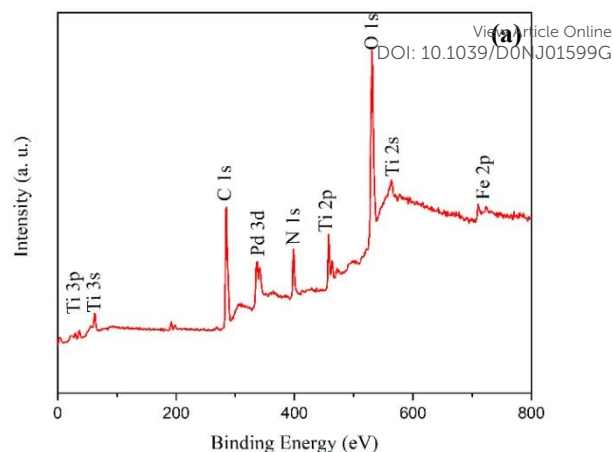
Figure 1. Overall flowchart for the fabrication of  $g\text{-C}_3\text{N}_4/\gamma\text{-Fe}_2\text{O}_3/\text{TiO}_2/\text{Pd}$ .

FT-IR spectra of  $g\text{-C}_3\text{N}_4$ ,  $\gamma\text{-Fe}_2\text{O}_3$  and  $g\text{-C}_3\text{N}_4/\gamma\text{-Fe}_2\text{O}_3/\text{TiO}_2$  are shown in Figure 2. In the FT-IR spectrum of  $g\text{-C}_3\text{N}_4$  (Figure 2a), the intense adsorption band at around  $808\text{ cm}^{-1}$  is ascribed to the breathing mode of triazine units.<sup>50</sup> The strong adsorption bands at about  $1238\text{--}1641\text{ cm}^{-1}$  could correspond to the stretching vibration frequencies of both aromatic C–N and C=N bonds.<sup>51</sup> The observed broad band at around  $3000\text{--}3450\text{ cm}^{-1}$  could attribute to the stretching vibration frequency of the NH and  $\text{NH}_2$  groups.<sup>52</sup> The FT-IR spectrum of  $\gamma\text{-Fe}_2\text{O}_3$  (Figure 2b) exhibited a wide absorption band at about  $542\text{--}695\text{ cm}^{-1}$ , which is related to the vibration mods of Fe–O bonds in the  $\gamma\text{-Fe}_2\text{O}_3$  crystalline lattice.<sup>49</sup> The characteristic bands appeared at  $1617$  and  $3406\text{ cm}^{-1}$  are in turn certified to the bending and stretching vibrations of the surface hydroxyl groups and adsorbed water molecules.<sup>53</sup> As it can be seen in the FT-IR spectrum of  $g\text{-C}_3\text{N}_4/\gamma\text{-Fe}_2\text{O}_3/\text{TiO}_2$  (Figure 2c), the broad characteristic stretching vibration band of Ti–O at  $498\text{--}769$ , which overlapped with the stretching vibrations of Fe–O bond is obvious. Moreover, the major characteristic bands of  $g\text{-C}_3\text{N}_4$  could be easily detected in the  $g\text{-C}_3\text{N}_4/\gamma\text{-Fe}_2\text{O}_3/\text{TiO}_2$  spectrum.



**Figure 2.** FT-IR spectra of (a)  $g\text{-C}_3\text{N}_4$ ; (b)  $\gamma\text{-Fe}_2\text{O}_3$  and (c)  $g\text{-C}_3\text{N}_4/\gamma\text{-Fe}_2\text{O}_3/\text{TiO}_2$ .

XPS was performed to investigate the electronic features and elemental composition of  $g\text{-C}_3\text{N}_4/\gamma\text{-Fe}_2\text{O}_3/\text{TiO}_2/\text{Pd}$  (Figure 3). As it is depicted in Figure 3a, the presence of the distinct characteristic peaks corresponding to C, N, O, Ti, Fe, and Pd is confirmed in the XPS elemental survey of the catalyst. Figure 3b showed the high-resolution XPS spectrum of C 1s in  $g\text{-C}_3\text{N}_4/\gamma\text{-Fe}_2\text{O}_3/\text{TiO}_2/\text{Pd}$ , which is deconvoluted into four main peaks. The peak observed at 284.6 eV could assign to the adventitious C-C bonds.<sup>54</sup> The signals observed at 285.8, 287.6 and 288.8 eV are related to the  $sp^2$  carbon atoms in the C-N-C, N=C-(N)<sub>2</sub>, N=C(N)-NH<sub>2</sub> and N=C(N)-NH groups.<sup>9,54</sup> The high resolution of N 1s spectrum revealed three indicative peaks centered at 398.4, 399.7, and 400.9 eV, corresponding to the  $sp^2$  nitrogen atoms (C-N=C),  $sp^3$  nitrogen atoms [H-N-(C)<sub>3</sub>] and amino groups (C-NH<sub>x</sub>), respectively.<sup>55–57</sup> In the Ti 2p spectrum of the catalyst (Figure 3d), two strong peaks with binding energies of about 458.0 and 463.9 eV relating to Ti 2p<sub>3/2</sub> and Ti 2p<sub>1/2</sub> could attribute to Ti<sup>4+</sup> in TiO<sub>2</sub> lattice.<sup>52</sup> The high-resolution XPS spectrum of Fe 2p (Figure 3e) illustrated four dominant peaks at 710.1 and 712.4 eV (Fe 2p<sub>3/2</sub>), and 723.9 and 725.2 eV (Fe 2p<sub>1/2</sub>), which evidenced the existence of Fe<sup>3+</sup> ions.<sup>58–60</sup> The fitted Fe 2p<sub>3/2</sub> peak at 710.1 eV, can be allocated to Fe<sup>3+</sup> state in the Ti-O-Fe bond.<sup>58</sup> The presence of a satellite peak at 718.2 eV is characteristic for Fe<sup>3+</sup> ions in  $\gamma\text{-Fe}_2\text{O}_3$ .<sup>60</sup> The absence of the Fe 2p<sub>3/2</sub> peak at 709.3 eV suggested that any Fe<sup>2+</sup> did not exist in the synthesized catalyst.<sup>58</sup> In the XPS spectrum of Pd (Figure 3f), the presence of binding energies at 335.1 and 336.5 eV (Pd 3d<sub>5/2</sub>) alongside the binding energies at 340.2 and 341.6 eV (Pd 3d<sub>3/2</sub>) could ascribe to Pd with zero oxidation state.<sup>5,61,62</sup> Furthermore, the other two minor peaks centered at 337.9 and 343.06 eV are attributed to Pd (II) 3d<sub>5/2</sub> and 3d<sub>3/2</sub>, respectively.<sup>61,63</sup> The ratio of Pd (0) to Pd (II) is about 3:1, which indicates that Pd species in the catalyst mainly exist in the zero-valent form.





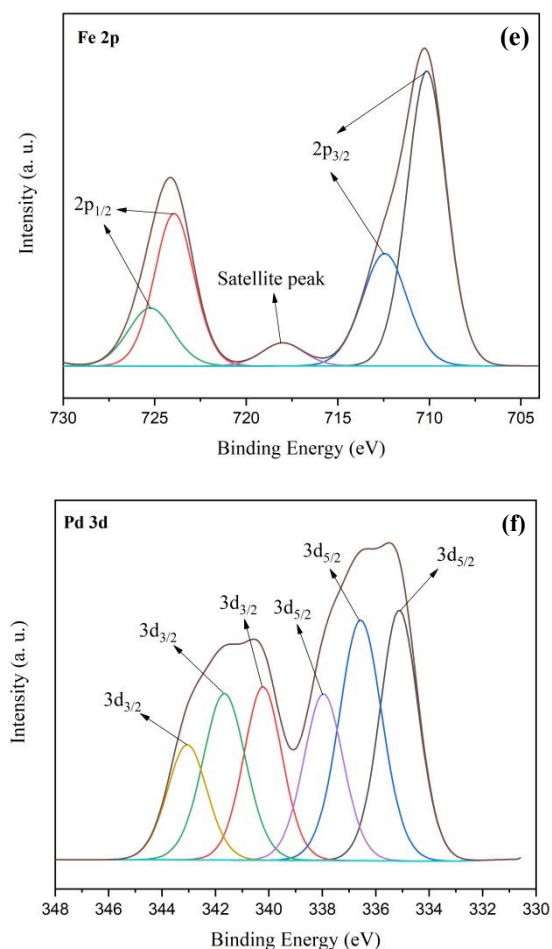


**Figure 3.** (a) XPS elemental survey spectrum, and high resolution XPS spectra of (b) C 1s, (c) N 1s, (d) Ti 2p, (e) Fe 2p and (f) Pd 3d of  $g\text{-C}_3\text{N}_4/\gamma\text{-Fe}_2\text{O}_3/\text{TiO}_2/\text{Pd}$ .

The Pd content of the photocatalyst was measured by ICP analysis, which showed the presence of 0.19 mmol Pd per 1.0 g of the  $g\text{-C}_3\text{N}_4/\gamma\text{-Fe}_2\text{O}_3/\text{TiO}_2/\text{Pd}$ .

XRD analysis was carried out for  $\gamma\text{-Fe}_2\text{O}_3$  and  $g\text{-C}_3\text{N}_4/\gamma\text{-Fe}_2\text{O}_3/\text{TiO}_2$  to understand the structural features of the catalyst (see the details in ESI, Figure S1).

The surface morphology of  $g\text{-C}_3\text{N}_4/\gamma\text{-Fe}_2\text{O}_3/\text{TiO}_2/\text{Pd}$  was further determined using SEM and TEM images. In Figure 4,  $g\text{-C}_3\text{N}_4$  sheets accompanied with the spherical nanoparticles can be seen. As it is clear in the TEM images, the mean particle sizes of  $\gamma\text{-Fe}_2\text{O}_3$  and  $\text{TiO}_2$  were measured to be around 12-17 nm. Comparison of the TEM images of  $g\text{-C}_3\text{N}_4/\gamma\text{-Fe}_2\text{O}_3/\text{TiO}_2/\text{Pd}$  with that of  $g\text{-C}_3\text{N}_4/\gamma\text{-Fe}_2\text{O}_3/\text{TiO}_2$ , clearly showed the presence of smaller nanoparticles in the TEM images of  $g\text{-C}_3\text{N}_4/\gamma\text{-Fe}_2\text{O}_3/\text{TiO}_2/\text{Pd}$ , which could be referred to Pd NPs with the particle sizes of about 2-5 nm. The particles of  $\gamma\text{-Fe}_2\text{O}_3$  and  $\text{TiO}_2$  can also be recognized through their indicative crystal lattice fringes<sup>64-66</sup> (Figure 4g). Moreover, the homogenous nature of the photocatalyst is visible at low magnification (Figure 4h).

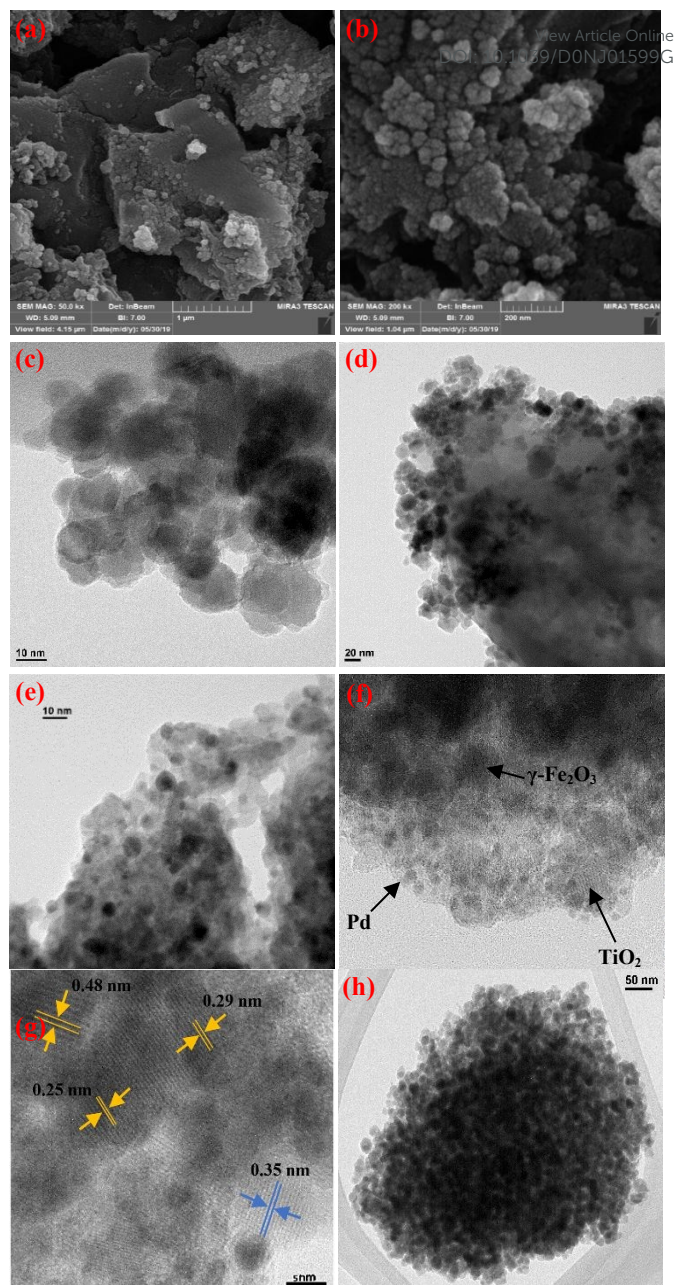


**Figure 4.** (a, b) SEM images of  $g\text{-C}_3\text{N}_4/\gamma\text{-Fe}_2\text{O}_3/\text{TiO}_2/\text{Pd}$ , and TEM images of (c)  $g\text{-C}_3\text{N}_4/\gamma\text{-Fe}_2\text{O}_3/\text{TiO}_2$  and (d-h)  $g\text{-C}_3\text{N}_4/\gamma\text{-Fe}_2\text{O}_3/\text{TiO}_2/\text{Pd}$ .

Moreover, an elemental mapping analysis was presented to more insight to the elemental composition of the catalyst (see the details in ESI, Figure S2).

The magnetic behavior of  $\gamma\text{-Fe}_2\text{O}_3$  and  $g\text{-C}_3\text{N}_4/\gamma\text{-Fe}_2\text{O}_3/\text{TiO}_2/\text{Pd}$  was examined by VSM analysis at room temperature (Figure 5). As it could be perceived from the resulting magnetization curves, the saturation magnetization amount of  $\gamma\text{-Fe}_2\text{O}_3$  and  $g\text{-C}_3\text{N}_4/\gamma\text{-Fe}_2\text{O}_3/\text{TiO}_2/\text{Pd}$  were 66.50 and 24.30  $\text{emu}\cdot\text{g}^{-1}$ , respectively. No detected hysteresis loop in the magnetization curves of both  $\gamma\text{-Fe}_2\text{O}_3$  and  $g\text{-C}_3\text{N}_4/\gamma\text{-Fe}_2\text{O}_3/\text{TiO}_2/\text{Pd}$  indicated the superparamagnetic feature of these compounds.

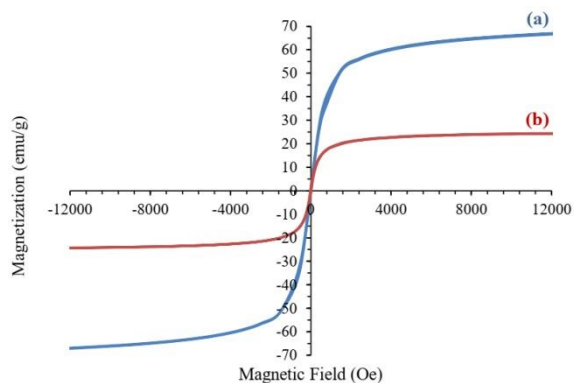


**Figure 5.** Magnetization curves of (a)  $\gamma$ -Fe<sub>2</sub>O<sub>3</sub> and (b) g-C<sub>3</sub>N<sub>4</sub>/ $\gamma$ -Fe<sub>2</sub>O<sub>3</sub>/TiO<sub>2</sub>/Pd.

The comparative UV-vis diffuse reflectance spectra of the as-prepared g-C<sub>3</sub>N<sub>4</sub>/ $\gamma$ -Fe<sub>2</sub>O<sub>3</sub>/TiO<sub>2</sub>/Pd and g-C<sub>3</sub>N<sub>4</sub>/ $\gamma$ -Fe<sub>2</sub>O<sub>3</sub>/TiO<sub>2</sub> are shown in Figure 6. As it is obvious, the g-C<sub>3</sub>N<sub>4</sub>/ $\gamma$ -Fe<sub>2</sub>O<sub>3</sub>/TiO<sub>2</sub> displayed a great absorption in the visible light area (Figure 6a). However, an even stronger absorption in the whole visible light region for the g-C<sub>3</sub>N<sub>4</sub>/ $\gamma$ -Fe<sub>2</sub>O<sub>3</sub>/TiO<sub>2</sub> modified with Pd NPs, indicated that the visible light energy can be better exploited by g-C<sub>3</sub>N<sub>4</sub>/ $\gamma$ -Fe<sub>2</sub>O<sub>3</sub>/TiO<sub>2</sub>/Pd as a photocatalyst (Figure 6b).

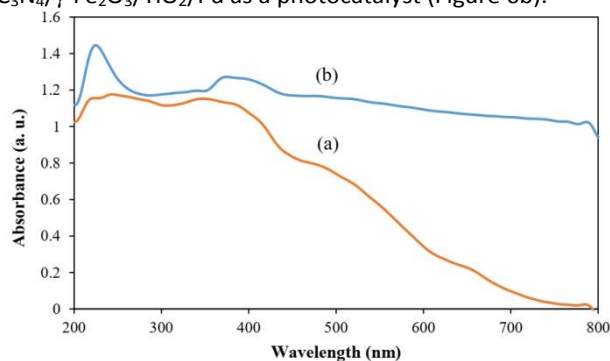


**Figure 6.** UV-vis diffuse reflectance spectrum of (a) g-C<sub>3</sub>N<sub>4</sub>/ $\gamma$ -Fe<sub>2</sub>O<sub>3</sub>/TiO<sub>2</sub> and (b) g-C<sub>3</sub>N<sub>4</sub>/ $\gamma$ -Fe<sub>2</sub>O<sub>3</sub>/TiO<sub>2</sub>/Pd.

### The photocatalytic activity of g-C<sub>3</sub>N<sub>4</sub>/ $\gamma$ -Fe<sub>2</sub>O<sub>3</sub>/TiO<sub>2</sub>/Pd in the fluoride-free Hiyama cross-coupling reaction

The influence of some critical reaction conditions in the Hiyama cross-coupling reaction was evaluated in the presence of g-C<sub>3</sub>N<sub>4</sub>/ $\gamma$ -Fe<sub>2</sub>O<sub>3</sub>/TiO<sub>2</sub>/Pd as a photocatalyst (Table 1). In this regard, the coupling reaction of iodobenzene with triethoxyphenylsilane was chosen as the benchmark reaction and the effect of various factors including different solvents, bases, catalyst amounts, and visible light sources were explored towards the reaction progress. Among the several solvents

screened for this transformation (Table 1, entries 1-8), the best yield of the product was obtained in EtOH (Table 1, entry 2). Thereafter, the effects of different bases on the reaction progress were investigated in EtOH (Table 1, entries 9-13) and results revealed that the best yield of the product was obtained in the presence of NaOH (Table 1, entry 2). However, the reaction did not proceed without utilizing any base (Table 1, entry 14). The effect of the photocatalyst amount was next studied (Table 1, entries 15-17). As clearly understood from the results in Table 1, a superior yield of the desired product was achieved by using 0.07 mol% of the photocatalyst (Table 1, entry 2). A control experiment revealed that no product was obtained when the reaction was performed in the absence of the catalyst (Table 1, entry 18). To obtain better insight into the catalytic efficiency of g-C<sub>3</sub>N<sub>4</sub>/ $\gamma$ -Fe<sub>2</sub>O<sub>3</sub>/TiO<sub>2</sub>/Pd, the photocatalytic activity of g-C<sub>3</sub>N<sub>4</sub>,  $\gamma$ -Fe<sub>2</sub>O<sub>3</sub>, g-C<sub>3</sub>N<sub>4</sub>/ $\gamma$ -Fe<sub>2</sub>O<sub>3</sub>/TiO<sub>2</sub>, and g-C<sub>3</sub>N<sub>4</sub>/Pd were separately studied in the model reaction (Table 1, entries 19-22). As can be seen in Table 1, no product was gained by using g-C<sub>3</sub>N<sub>4</sub>,  $\gamma$ -Fe<sub>2</sub>O<sub>3</sub>, and g-C<sub>3</sub>N<sub>4</sub>/ $\gamma$ -Fe<sub>2</sub>O<sub>3</sub>/TiO<sub>2</sub> species. However, when the reaction was carried out in the presence of g-C<sub>3</sub>N<sub>4</sub>/Pd, the result was far from satisfactory (Table 1, entry 22). These findings indicated that the enhanced photocatalytic activity of g-C<sub>3</sub>N<sub>4</sub>/ $\gamma$ -Fe<sub>2</sub>O<sub>3</sub>/TiO<sub>2</sub>/Pd could be attributed to the synergistic catalytic effect of Pd NPs and g-C<sub>3</sub>N<sub>4</sub>/ $\gamma$ -Fe<sub>2</sub>O<sub>3</sub>/TiO<sub>2</sub> towards the Hiyama cross-coupling reaction (see the photocatalytic mechanism part for more details). It can be supposed that the convenient combination of g-C<sub>3</sub>N<sub>4</sub>,  $\gamma$ -Fe<sub>2</sub>O<sub>3</sub> and TiO<sub>2</sub> in the nanocomposite, not only promotes the visible light-harvesting capacity of the catalyst but also facilitates the high electron conductivity within the nanocomposite structure. This property enables the charge separation and lengthens the lifetime of photogenerated electron-hole pairs by reducing the recombination rate. Pd NPs as the electron reservoir can trap the photogenerated electrons<sup>45</sup> and well expedite the cross-coupling reactions under visible light irradiation. The effect of different light sources was also examined on the model reaction progress (Table 1, entries 23-26) and found that the cross-coupling reaction proceeded surprisingly under the white LED illumination (12 W) (Table 1, entry 2). It is worth to note that the coupling reaction did not proceed at all in dark conditions (entry 27). These observations well proved the significant influence of the light irradiation to advance the Hiyama cross-coupling reaction. In the next experiment, white LED lamps with different intensities were separately used to investigate the effect of light intensity on the progress of the model reaction (Table 1, entries 28-30). Results indicated that a 12 W white LED lamp is the best light source for the Hiyama cross-coupling reaction (Table 1, entry 2).

**Table 1.** Screening the reaction conditions for visible-light-promoted fluoride-free Hiyama cross-coupling reaction of iodobenzene with triethoxyphenylsilane in the presence of g-C<sub>3</sub>N<sub>4</sub>/ $\gamma$ -Fe<sub>2</sub>O<sub>3</sub>/TiO<sub>2</sub>/Pd.

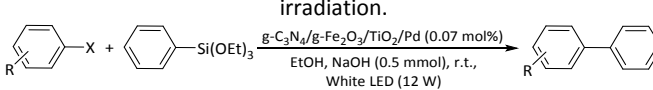
Entry	Solvent	Catalyst (mol%)	Base	Light Source	Time (h)	Isolated Yield <sup>a</sup> (%)
1	H <sub>2</sub> O	0.07	NaOH	White LED (12 W)	4	22
2	EtOH	0.07	NaOH	White LED (12 W)	2	97
3	H <sub>2</sub> O-EtOH	0.07	NaOH	White LED (12 W)	4	73

4	DMF	0.07	NaOH	White LED (12 W)	7	15
5	EtOAc	0.07	NaOH	White LED (12 W)	7	25
6	CH <sub>3</sub> CN	0.07	NaOH	White LED (12 W)	11	30
7	Toluene	0.07	NaOH	White LED (12 W)	3	Trace
8	HOAc	0.07	NaOH	White LED (12 W)	3	65
9	EtOH	0.07	Et <sub>3</sub> N	White LED (12 W)	5	76
10	EtOH	0.07	K <sub>2</sub> CO <sub>3</sub>	White LED (12 W)	4	82
11	EtOH	0.07	Cs <sub>2</sub> CO <sub>3</sub>	White LED (12 W)	4.5	78
12	EtOH	0.07	K <sub>3</sub> PO <sub>4</sub>	White LED (12 W)	6	65
13	EtOH	0.07	KF	White LED (12 W)	4	67
14	EtOH	0.07	-	White LED (12 W)	10	0
15	EtOH	0.06	NaOH	White LED (12 W)	5	95
16	EtOH	0.08	NaOH	White LED (12 W)	2	97
17	EtOH	0.09	NaOH	White LED (12 W)	8	88
18	EtOH	0	NaOH	White LED (12 W)	24	0
19	EtOH	0.07 <sup>b</sup>	NaOH	White LED (12 W)	24	0
20	EtOH	0.07 <sup>c</sup>	NaOH	White LED (12 W)	24	0
21	EtOH	0.07 <sup>d</sup>	NaOH	White LED (12 W)	24	0
22	EtOH	0.07 <sup>e</sup>	NaOH	White LED (12 W)	24	47
23	EtOH	0.07	NaOH	Blue LED (12 W)	2	90
24	EtOH	0.07	NaOH	Green LED (12 W)	12	50
25	EtOH	0.07	NaOH	Room light	5	Trace
26	EtOH	0.07	NaOH	Sunlight <sup>f</sup>	6	60
27	EtOH	0.07	NaOH	Dark	24	0
28	EtOH	0.07	NaOH	White LED (5 W)	2	15
29	EtOH	0.07	NaOH	White LED (10 W)	2	65
30	EtOH	0.07	NaOH	White LED (20 W)	2	97

<sup>a</sup>Reaction conditions: Iodobenzene (1 mmol), triethoxyphenylsilane (1 mmol), base (0.5 mmol), g-C<sub>3</sub>N<sub>4</sub>/γ-Fe<sub>2</sub>O<sub>3</sub>/TiO<sub>2</sub>/Pd (except for entries 3, 21-24), and solvent (4 mL), under visible light irradiation. The reaction vial was submerged in a water bath at 25 °C to avoid the photothermal effect.; <sup>b</sup>Reaction was performed in the presence of g-C<sub>3</sub>N<sub>4</sub> as the catalyst; <sup>c</sup>Reaction was performed in the presence of γ-Fe<sub>2</sub>O<sub>3</sub> as the catalyst; <sup>d</sup>Reaction was performed in the presence of g-C<sub>3</sub>N<sub>4</sub>/γ-Fe<sub>2</sub>O<sub>3</sub>/TiO<sub>2</sub> as the catalyst; <sup>e</sup>Reaction was performed in the presence of g-C<sub>3</sub>N<sub>4</sub>/Pd as the catalyst; <sup>f</sup>This experiment was executed between 9:00 and 15:00 h, in a summer day in Birjand city, at room temperature (25 °C).

With the optimized reaction conditions in hand, the scope of the fluoride-free Hiyama cross-coupling reaction was extended to various aryl halides with triethoxyphenylsilane under the visible light irradiation (Table 2). As depicted in Table 2, a variety of aryl iodides/bromides (Entries 1-9) and even chlorides (Entries 10-13) as the highly challenging substrates which are far extensively available and cheaper than aryl iodides and bromides, underwent the cross-coupling reaction with triethoxyphenylsilane and the desired products were obtained in good to high yields. Importantly, any homocoupling product was not detected in all of these reactions.

**Table 2.** Substrate scope for the fluoride-free Hiyama cross-coupling reaction catalyzed by g-C<sub>3</sub>N<sub>4</sub>/γ-Fe<sub>2</sub>O<sub>3</sub>/TiO<sub>2</sub>/Pd under visible-light



Entry	X	R	Time (h)	Isolated Yield <sup>a</sup> (%)
1	I	H	2	97
2	I	4-I	5	88
3	I	4-OMe	7	90
4	I	4-Cl	1.5	96
5	Br	H	3.5	95
6	Br	4-NO <sub>2</sub>	3	98
7	Br	4-OMe	10	86
8	Br	4-Cl	3	90
9	Br	4-CN	3	89



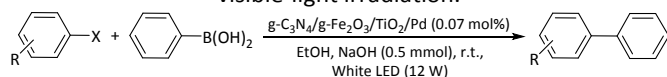
10	Cl	H	6	90
11	Cl	4-NO <sub>2</sub>	4	85
12	Cl	4-CN	4.5	80
13	Cl	4-OMe	12	79

<sup>a</sup>Reaction conditions: aryl halide (1 mmol), triethoxyphenylsilane (1 mmol), NaOH (0.5 mmol), g-C<sub>3</sub>N<sub>4</sub>/γ-Fe<sub>2</sub>O<sub>3</sub>/TiO<sub>2</sub>/Pd (0.07 mol%), in EtOH (4 mL) under white LED irradiation (12 W). The reaction vial was submerged in a water bath at 25 °C to avoid the photothermal effect.

### The photocatalytic activity of g-C<sub>3</sub>N<sub>4</sub>/γ-Fe<sub>2</sub>O<sub>3</sub>/TiO<sub>2</sub>/Pd in Suzuki–Miyaura cross-coupling reaction

Encouraged by the promising results obtained from the fluoride-free Hiyama cross-coupling reaction, the photocatalytic activity of g-C<sub>3</sub>N<sub>4</sub>/γ-Fe<sub>2</sub>O<sub>3</sub>/TiO<sub>2</sub>/Pd was next explored towards the Suzuki–Miyaura cross-coupling reaction under visible light irradiation (Table 3). As shown in Table 3, this photocatalytic method was very efficient for the cross-coupling reaction of different aryl iodides and bromides with phenylboronic acid (Entries 1-9). Interestingly, it was found that the cross-coupling reactions for the easily available and low-cost aryl chlorides as the highly challenging substrates, with phenylboronic acid, were also accompanied with satisfactory results (Table 3, entries 10-13).

**Table 3.** Substrate scope for the Suzuki–Miyaura cross-coupling reaction catalyzed by g-C<sub>3</sub>N<sub>4</sub>/γ-Fe<sub>2</sub>O<sub>3</sub>/TiO<sub>2</sub>/Pd under visible-light irradiation.



Entry	X	R	Time (h)	Isolated Yield <sup>a</sup> (%)
1	I	H	30 min	98
2	I	4-I	1.5	92
3	I	4-OMe	1.5	88
4	I	4-Cl	20 min	98
5	Br	H	45 min	91
6	Br	4-NO <sub>2</sub>	2.5	98
7	Br	4-OMe	4	87
8	Br	4-Cl	1.5	94
9	Br	4-CN	2.5	95
10	Cl	H	3	91
11	Cl	4-NO <sub>2</sub>	1	87
12	Cl	4-CN	4	83
13	Cl	4-OMe	7	80

<sup>a</sup>Reaction conditions: aryl halide (1 mmol), boronic acid (1 mmol), NaOH (0.5 mmol), g-C<sub>3</sub>N<sub>4</sub>/γ-Fe<sub>2</sub>O<sub>3</sub>/TiO<sub>2</sub>/Pd (0.07 mol%), in EtOH (4 mL) under white LED irradiation (12 W). The reaction vial was submerged in a water bath at 25 °C to avoid the photothermal effect.

### The stability and reusability of g-C<sub>3</sub>N<sub>4</sub>/γ-Fe<sub>2</sub>O<sub>3</sub>/TiO<sub>2</sub>/Pd as a photocatalyst in the Hiyama and Suzuki–Miyaura cross-coupling reactions

Recovery and reusability of the photocatalyst are very significant factors, particularly for commercial and industrial applications. These capabilities, clearly assert a heterogeneous catalyst as a suitable candidate towards more sustainable and green chemical

developments. In this line, to investigate the photocatalyst recyclability, a set of experiments were performed for the model Hiyama and Suzuki–Miyaura cross-coupling reactions, under the optimized reaction conditions. To do this, after each run of the experiment, the catalyst was separated from the reaction mixture through the magnetic decantation. Then, the isolated catalyst was washed with water and EtOH, vacuum-dried at 50 °C for 2 h, and directly used in the next run of the reaction. As it can be seen in Figure 7, in both Hiyama and Suzuki–Miyaura cross-coupling reactions, g-C<sub>3</sub>N<sub>4</sub>/γ-Fe<sub>2</sub>O<sub>3</sub>/TiO<sub>2</sub>/Pd exhibited high photocatalytic activity in seven successive runs, which suggested the appreciated durability of the catalyst.

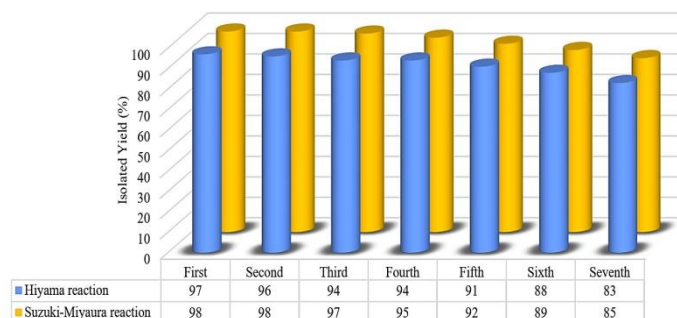


**Figure 7.** Recyclability of g-C<sub>3</sub>N<sub>4</sub>/γ-Fe<sub>2</sub>O<sub>3</sub>/TiO<sub>2</sub>/Pd in the model Hiyama and Suzuki–Miyaura cross-coupling reactions, under the optimized reaction conditions; Reaction times: 2 h (Hiyama cross-coupling reaction) and 30 min (Suzuki–Miyaura cross-coupling reaction).

The FT-IR spectrum of the recovered catalyst after seven runs (Figure 8), revealed the entire preservation of the shape, position and relative intensity of the characteristic absorption bands. This result clearly proved that no substantial changes occurred in the chemical structure of the present catalyst.

Furthermore, the XPS analysis of the recycled g-C<sub>3</sub>N<sub>4</sub>/γ-Fe<sub>2</sub>O<sub>3</sub>/TiO<sub>2</sub>/Pd after seven runs indicated the preservation of electronic features for all elements (Figure 9). These findings well suggested the commendable stability and durability of the photocatalyst.

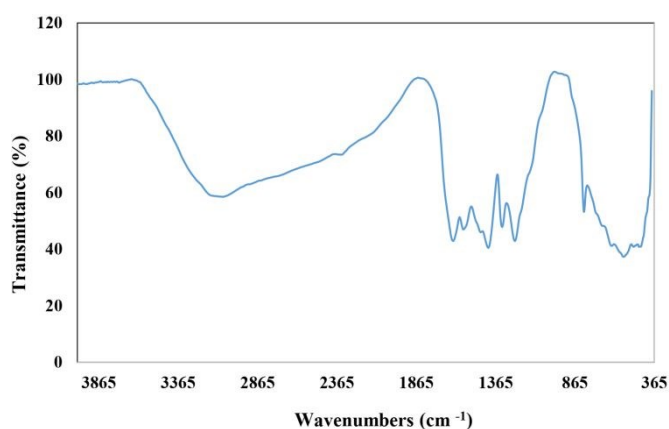


**Figure 8.** The FT-IR spectrum of g-C<sub>3</sub>N<sub>4</sub>/γ-Fe<sub>2</sub>O<sub>3</sub>/TiO<sub>2</sub> after 7<sup>th</sup> runs.



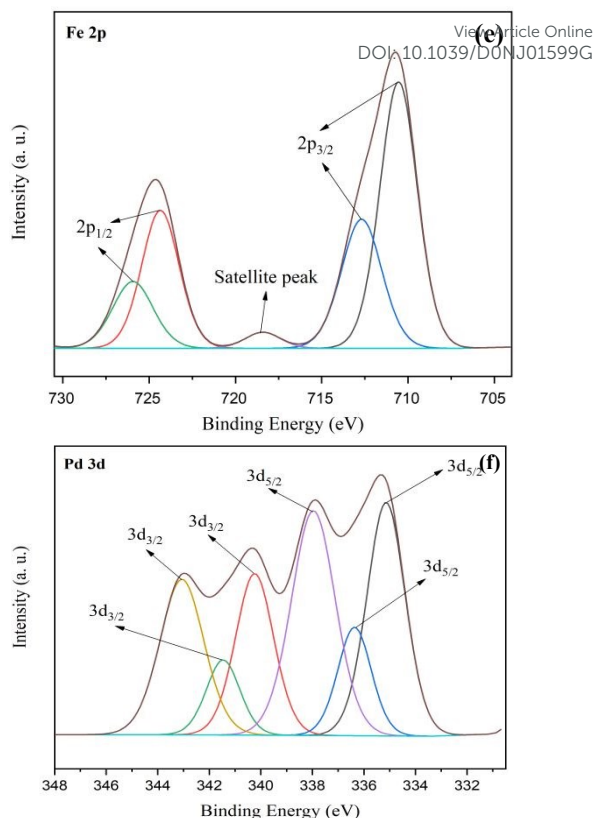
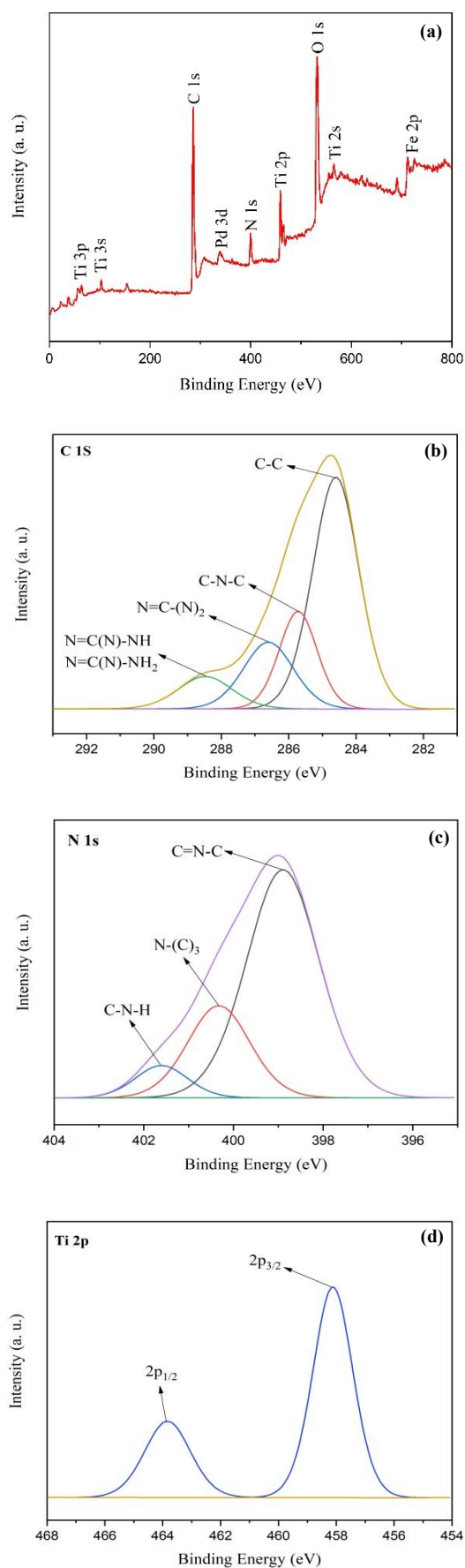


**Figure 9.** (a) XPS elemental survey spectrum, and high resolution XPS spectra of (b) C 1s, (c) N 1s, (d) Ti 2p, (e) Fe 2p and (f) Pd 3d of  $g\text{-C}_3\text{N}_4/\gamma\text{-Fe}_2\text{O}_3/\text{TiO}_2/\text{Pd}$  after 7<sup>th</sup> runs.

The comparison of the TEM images of the reused catalyst (Figure 10 a, b) with those of the fresh one (Figure 4d-h), suggested that the structure, morphology and the average nanoparticles size in the reused catalyst remained intact even after seven runs of the reaction.

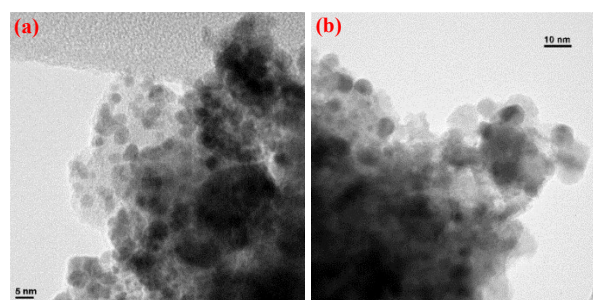


**Figure 10.** TEM images of the  $g\text{-C}_3\text{N}_4/\gamma\text{-Fe}_2\text{O}_3/\text{TiO}_2/\text{Pd}$  after seven runs.

The filtration test and poisoning experiment were performed to clarify the real heterogeneous nature of the catalyst. To conduct the filtration test, the model Hiyama cross-coupling reaction was carried out under the optimal reaction conditions. When 50% of the Hiyama cross-coupling reaction proceeded, the catalyst was separated from the reaction mixture and the filtrate was permitted to stir for further 10 h. No more reaction progress well suggested the absence of any homogeneous catalyst in the reaction mixture (Figure 11b). ICP analysis of the filtrate also indicated a negligible amount of the Pd (<

0.1% of the total Pd content). For performing the poisoning experiment, the model Hiyama cross-coupling reaction was carried out in the presence of 3-mercaptopropyl functionalized  $\gamma$ -Fe<sub>2</sub>O<sub>3</sub> as an efficient Pd scavenger. As apparently illustrated in Figure 11c, any considerable change in the reaction progress was not observed by using Pd scavenger. Based on these observations, it can be concluded that the catalyst operated truly in a heterogeneous manner and it is completely stable under the reaction conditions.

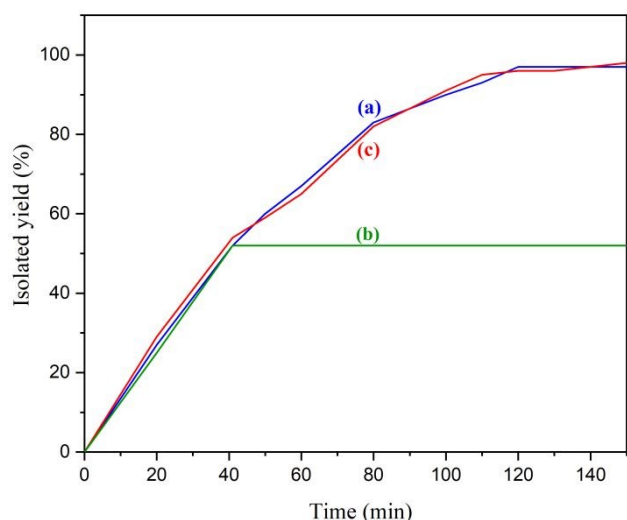
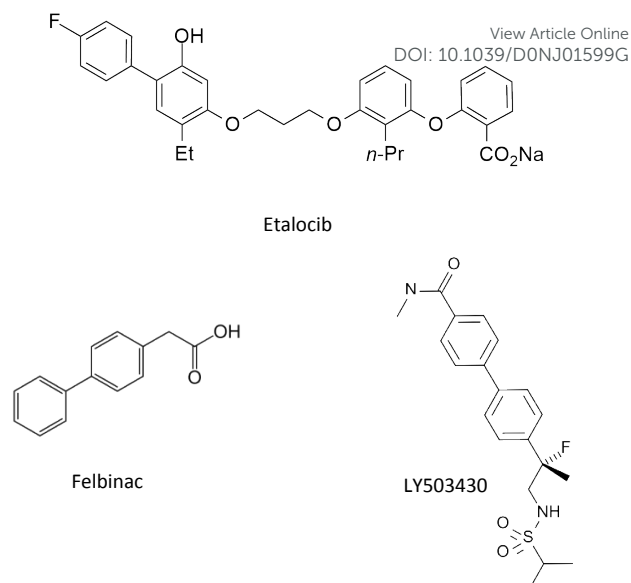
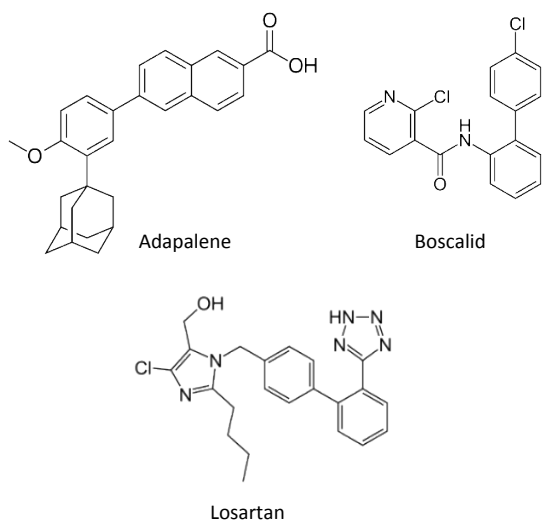


**Figure 11.** Reaction progress as a function of time for the model Hiyama cross-coupling reaction in (a) normal condition, (b) filtration test and (c) poisoning experiment.

### Large scale studies of cross-coupling reaction in the presence of $g$ -C<sub>3</sub>N<sub>4</sub>/ $\gamma$ -Fe<sub>2</sub>O<sub>3</sub>/TiO<sub>2</sub>/Pd as a photocatalyst

The resulting biaryl moieties have extensive applications as the fundamental building blocks in various fields of the chemical manufacturing industries.<sup>67</sup> For instance, the biaryl core is a vital segment in the structure of numerous drugs and pharmaceutical intermediates such as *Adapalene* (treatment of acne), *Boscalid* (fungicide), *Losartan* (anti-hypertensive), *Etalocib* (anti-cancer), *Felbinac* (anti-inflammatory), and *LY503430* (anti-Parkinson's)<sup>68,69</sup> (Scheme 1).



**Scheme 1.** Structure of some drugs with biaryl core.

One of the most common synthetic protocols for preparing functionalized biaryl derivatives is the Hiyama cross-coupling reactions of aryl siloxanes with aryl halides.<sup>15</sup> Therefore, by considering the particular importance of developing the industrial applications of biaryls, in the next experiment, we have established a large-scale Hiyama cross-coupling reaction. In this regard, the coupling reaction of iodobenzene with triethoxyphenylsilane in a scaled-up procedure (50 times) in the presence of  $g$ -C<sub>3</sub>N<sub>4</sub>/ $\gamma$ -Fe<sub>2</sub>O<sub>3</sub>/TiO<sub>2</sub>/Pd was accomplished successfully under the optimized reaction conditions. Interestingly, the scaled-up coupling reaction was associated with a 93% isolated yield of the desired biphenyl.

### Comparative study

To further elucidate the merits of the current photocatalytic system over the reported Pd-based photocatalytic systems in the Hiyama and Suzuki–Miyaura cross-coupling reactions, the comparing efficacy results were tabulated in Table 4. It can be seen that the present catalyst is much superior to almost all of the reported catalysts not only for the convenient reaction conditions, shorter reaction times, more reaction efficiency and lower catalyst loading but also in terms of the convenient magnetic catalyst recovery and reasonable reusability. More importantly, using an inexpensive eco-benign visible light source and no need to use any additive or toxic solvent, well support the present methodology in a movement towards the green chemistry. Notably, while, most of the previously reported methods suffer from a lack of generality for the cross-coupling reactions of aryl chlorides, the title approach is very effective for such transformations.

**Table 4.** Comparison of the photocatalytic activity of g-C<sub>3</sub>N<sub>4</sub>/γ-Fe<sub>2</sub>O<sub>3</sub>/TiO<sub>2</sub>/Pd with other Pd-based photocatalyzed Hiyama and Suzuki-Miyaura cross-coupling reactions under visible light irradiation.

View Article Online  
DOI: 10.1039/D0NJ01599G

Entry	Reaction	Photocatalyst (amount)	Ar-X	Reaction conditions	Time (h)	Isolated Yield (%)
1 <sup>a</sup>	Hiyama	g-C <sub>3</sub> N <sub>4</sub> /γ-Fe <sub>2</sub> O <sub>3</sub> /TiO <sub>2</sub> /Pd (0.07 mol%)	I	EtOH, NaOH, r.t., White LED	1.5-7	88-97
			Br	lamp (12 W)	3-10	72-95
			Cl		4-12	79-90
2 <sup>31</sup>	Hiyama	Nano Pd/ZnO (925 × 10 <sup>-9</sup> mol%)	I	PhCH <sub>3</sub> , Cs <sub>2</sub> CO <sub>3</sub> , r.t., White LED	3-6	60-84
			Br	lamp (11 W)	60	17
			Cl		55	13
3 <sup>32</sup>	Hiyama	Au-Pd alloy NPs (0.7 mol%)	I	PhCH <sub>3</sub> , TBAF <sup>b</sup> , 45 °C, Halogen	24	10-86
			Br	lamp (0.45 W.cm <sup>-2</sup> )	24	23
4 <sup>a</sup>	Suzuki-Miyaura	g-C <sub>3</sub> N <sub>4</sub> /γ-Fe <sub>2</sub> O <sub>3</sub> /TiO <sub>2</sub> /Pd (0.07 mol%)	I	EtOH, NaOH, r.t., White LED	0.33-1.5	88-98
			Br	lamp (12 W)	0.75-4	87-98
			Cl		1-7	80-91
5 <sup>33</sup>	Suzuki-Miyaura	TiO <sub>2</sub> -AA <sup>c</sup> -Pd (0.15 mol %)	I	solvent free, Et <sub>3</sub> N, 70 °C, CFL	0.5-4	45-96
			Br	lamp (40 W)	3-5	82-94
			Cl		6	80
6 <sup>34</sup>	Suzuki-Miyaura	Ru-Pd bimetallic complex (1 mol%)	Br	EtOH, PPh <sub>3</sub> , K <sub>2</sub> CO <sub>3</sub> , Ar, r.t., Xe lamp (500 W)	6	5.2-12
7 <sup>35</sup>	Suzuki-Miyaura	Au-Pd nanostructure solution (0.33 mL)	I	NaOH, CTAB <sup>d</sup> , H <sub>2</sub> O, 30 °C, Sunlight	2	97
			Br		2	50-99
8 <sup>36</sup>	Suzuki-Miyaura	Au-Pd alloy NPs (3%)	I	DMF/H <sub>2</sub> O (3:1), K <sub>2</sub> CO <sub>3</sub> , Ar, 30 °C, Halogen lamp (0.5 W.cm <sup>-2</sup> )	2-22	23-100 <sup>f</sup>
			Br <sup>e</sup>		3	25-87 <sup>f</sup>
9 <sup>37</sup>	Suzuki-Miyaura	nano Pd/TiO <sub>2</sub> (0.015g, containing 7.04 × 10 <sup>-3</sup> mmol of Pd)	I	H <sub>2</sub> O-PEG (1:1), NaOC(CH <sub>3</sub> ) <sub>3</sub> , 28 °C, White LED (15 W)	4-6	62-98
			Br		6	51-96
			Cl		20	21-32
10 <sup>38</sup>	Suzuki-Miyaura	HUY@S-TOH <sup>g</sup> /AuPd (5.0 mg of catalyst, 0.6 wt% Pd)	I	EtOH/H <sub>2</sub> O (2:1), K <sub>2</sub> CO <sub>3</sub> , r.t., Xe lamp (300 W)	0.5-3	90-99
			Br		2-5	72-94
			Cl		7-8	61-65
11 <sup>31</sup>	Suzuki-Miyaura	Nano Pd/ZnO (925 × 10 <sup>-9</sup> mol%)	I	H <sub>2</sub> O, Cs <sub>2</sub> CO <sub>3</sub> , r.t., White LED	0.83-1.5	95-99
			Br	lamp (11 W)	0.75-5	71-99
			Cl		5-24	48-94

12 <sup>39</sup>	Suzuki-Miyaura	Pd/Au/PN <sup>h</sup> -CeO <sub>2</sub> (2.95 wt% Au, 0.41wt% Pd)	Cl	DMF/H <sub>2</sub> O (1:1), K <sub>2</sub> CO <sub>3</sub> , 25 °C; Xe lamp (150 W)	5	98.8
13 <sup>40</sup>	Suzuki-Miyaura	Pd@B-BO <sub>3</sub> (10 mg, 3 wt % Pd content)	I Br	DMF/H <sub>2</sub> O (1:1), K <sub>2</sub> CO <sub>3</sub> , r.t., White LED lamp (1.2 W.cm <sup>-2</sup> )	2-6 4-16	75-98 76-96
14 <sup>41</sup>	Suzuki-Miyaura	Pd/SiC (10 mg of catalyst, 3 wt% Pd)	I Br	DMF/H <sub>2</sub> O (3:1), Cs <sub>2</sub> CO <sub>3</sub> , Ar, 30 °C, Xe lamp (300 W, 0.35 W.cm <sup>-2</sup> )	1.33 1.33	53-99 93-100
15 <sup>42</sup>	Suzuki-Miyaura	GO-Pd@Ag-AgBr (25 mg)	I Br Cl	EtOH/H <sub>2</sub> O (1:1), K <sub>2</sub> CO <sub>3</sub> , N <sub>2</sub> , r.t., Xe lamp (300 W)	0.5 1-2 2	96-97 78-99 6
16 <sup>43</sup>	Suzuki-Miyaura	Pd@PDA-CL <sup>i</sup> (20 mg, 3 wt% Pd content)	I Br	DMF/H <sub>2</sub> O (1:1), K <sub>2</sub> CO <sub>3</sub> , r.t., White LED lamp (1.2 W.cm <sup>-2</sup> )	2 2	90-98 30-99
17 <sup>35</sup>	Suzuki-Miyaura	Au-Pd nanostructure solution (0.5 mL)	I Br	NaOH, CTAB, H <sub>2</sub> O, r.t., laser power (809 nm, 1.68 W)	1 1	99 43-99
18 <sup>44</sup>	Suzuki-Miyaura	Au-Pd/TiO <sub>2</sub> (0.2 mol%, 0.002 mmol Pd)	I Br Cl	H <sub>2</sub> O/EtOH (1:1), K <sub>2</sub> CO <sub>3</sub> , 25 °C, Blue LED lamp (5 W)	5 5 5	55-96 70 14
19 <sup>45</sup>	Suzuki-Miyaura	PdNiFe <sub>2</sub> O <sub>4</sub> /rGO (0.5 mmol% Pd)	I Br Cl	H <sub>2</sub> O/EtOH (1:9), K <sub>2</sub> CO <sub>3</sub> , N <sub>2</sub> , Xe lamp (300 W)	0.5-1 1.5 2-6	80-99 89-98 25-55
20 <sup>46</sup>	Suzuki-Miyaura	m-CNR <sup>j</sup> -Pd (10 mg of catalyst, 3 wt% Pd)	I	H <sub>2</sub> O/EtOH (1:1), K <sub>2</sub> CO <sub>3</sub> , r.t. Xe lamp (150 W)	1	99 <sup>f</sup>

<sup>a</sup> Present work; <sup>b</sup> Tetrabutyl ammonium fluoride; <sup>c</sup> Ascorbic acid; <sup>d</sup> Cetyl trimethylammonium bromide, <sup>e</sup> NaOH (3 mmol), CTAB (1 mmol), 10 mL H<sub>2</sub>O, 30 °C, 3 h, light intensity 0.5 W.cm<sup>-2</sup>; <sup>f</sup> Conversion; <sup>g</sup> hierarchical urchin-like yolk@shell TiO<sub>2</sub> architecture; <sup>h</sup> Porous Nanorods; <sup>i</sup> Polydopamine-carbonized loofah; <sup>j</sup> mesoporous g-C<sub>3</sub>N<sub>4</sub> nanorods.

### Photocatalytic mechanism

To find out a plausible mechanism for the photocatalytic Hiyama and Suzuki-Miyaura cross-coupling reactions in the presence of g-C<sub>3</sub>N<sub>4</sub>/γ-Fe<sub>2</sub>O<sub>3</sub>/TiO<sub>2</sub>/Pd, separate reactions between bromobenzene and phenylboronic acid/triethoxyphenylsilane were studied in the presence of electron and hole scavengers. When the reaction was carried out in the presence of 5,5-Dimethyl-1-pyrroline *N*-oxide (DMPO) as an electron-trapping agent to capture the electrons transferred from Pd NPs to bromobenzene, no target product was achieved. This result pointed to the fact that the lower the electron density of Pd NPs, the slower the speed of the oxidative addition step in both cross-coupling reactions.<sup>70</sup> Afterward, to study the role of photogenerated holes from the photocatalyst, triethanolamine

(TEOA) was employed as a hole scavenger in similar reactions to block the hole transfer to phenylboronic acid or triethoxyphenylsilane. It was observed that the reactions were entirely quenched. Indeed, stimulating the C-Si and C-B bond in Hiyama and Suzuki-Miyaura cross-coupling reactions, respectively) is an essential stage in the cross-coupling reactions that could be achieved *via* the photo-generated holes inside the photocatalyst.<sup>71</sup> These studies suggest that the photogenerated electron and hole pairs are crucial to conduct the photocatalytic Hiyama and Suzuki-Miyaura cross-coupling reactions. By analogy with these observations and reported mechanistic studies,<sup>38,45</sup> a plausible photocatalytic mechanism can be proposed for the Hiyama and Suzuki-Miyaura cross-coupling reactions over the g-C<sub>3</sub>N<sub>4</sub>/γ-Fe<sub>2</sub>O<sub>3</sub>/TiO<sub>2</sub>/Pd photocatalyst under visible light irradiation (Figure



12). Upon visible light irradiation, charge separation in the form of electron-hole pairs is generated in the  $g\text{-C}_3\text{N}_4/\gamma\text{-Fe}_2\text{O}_3/\text{TiO}_2/\text{Pd}$  as a photocatalyst. Then, the photo-induced electrons could be injected into the Pd NPs to increase the electron density of Pd. In fact, due to the electron reservoir capacity, Pd NPs can well trap the photogenerated electrons.<sup>43</sup> Subsequently, the electron-rich Pd NPs can activate the C-X bond of aryl halides ( $\text{Ar}^1\text{-X}$ ) and facilitates the oxidative addition step in both cross-coupling reactions.<sup>38,72</sup> On the other hand, arylboronic acid/triethoxyphenylsilane ( $\text{Ar}^2\text{-M}$ ) can acquire the  $\text{OH}^-$  ions in the basic reaction media to accelerate the

trans-metalation process.<sup>45</sup> Notably, based on the obtained results from the solvent screening studies (Table 1, entries 1-8), it can be hypothesized that the protic solvents may be oxidized easier than aprotic solvents through the photogenerated holes transferred from the photocatalyst.<sup>38,72</sup> Therefore, the photo-generated holes can diffuse to EtOH or can activate the  $\text{Ar}^2\text{-M}$  through the cleavage of the C-Si/C-B bond, to generate the biaryl-Pd NPs complex.<sup>38,62,72,73</sup> Finally, the cross-coupling reaction was completed *via* the reductive elimination step to furnish the desired product.

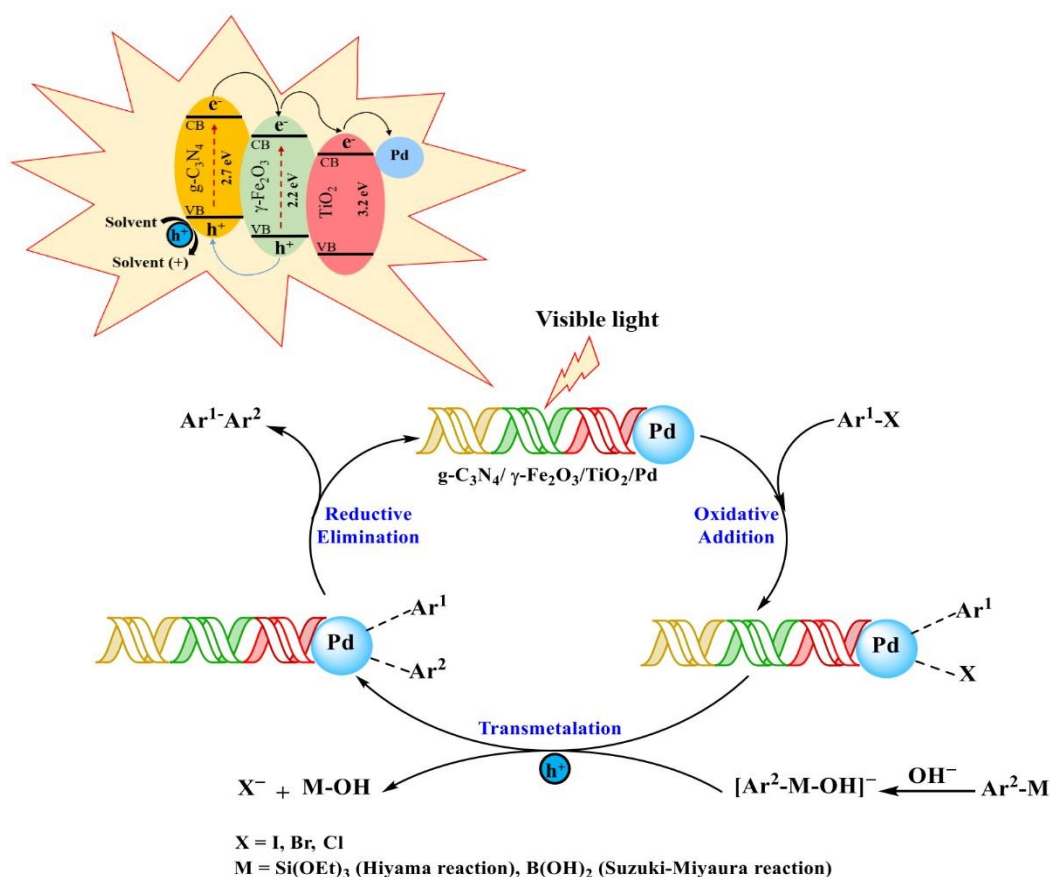


**Figure 12.** A plausible mechanism for the visible light induced photocatalytic Hiyama and Suzuki-Miyaura cross-coupling reactions catalyzed by  $g\text{-C}_3\text{N}_4/\gamma\text{-Fe}_2\text{O}_3/\text{TiO}_2/\text{Pd}$ .

## Experimental

### Materials and instruments

All chemicals and solvents were purchased from Merck chemical company and were used directly without further treatment. The purity of the products and the progress of the reactions were monitored using TLC on silica-gel Polygram SILG/UV254 plates. FT-IR spectra were recorded with a JASCO FT-IR 460 plus spectrophotometer within the 400-4000  $\text{cm}^{-1}$  range using KBr disc at room temperature. X-ray photoelectron spectroscopy (XPS) analyses were carried out using a VG-Microtech Multilab 3000 spectrometer, equipped with an Al anode. The deconvolution of spectra was carried out by using Gaussian Lorentzian curves. X-ray powder diffraction

(XRD) was carried out on an Xpert Pro Panalytical diffractometer with Cu  $\text{K}\alpha$  radiation ( $\lambda = 0.154 \text{ \AA}$ ). Scanning electron microscopy (SEM) and elemental mapping were performed using a TESCAN MIRA3 instrument. Transmission electron microscopy (TEM) was done using the TEM microscope JEOL JEM-1400 Plus. Room temperature magnetization isotherms were obtained using a homemade vibrating sample magnetometer (VSM) (Magnetic daghigh kavir, MDKB model, Iran). UV-vis diffuse reflectance spectroscopy (DRS) was conducted using a Shimadzu spectrophotometer (UV-2550 model). The content of palladium in the catalyst was determined with an OPTIMA 7300DV ICP analyzer. The NMR spectra were provided by Bruker Avance 300 and 400 MHz instruments in  $\text{CDCl}_3$  and  $\text{DMSO-}d_6$  in the presence of

tetramethylsilane as the internal standard and the coupling constants ( $J$  values) are given in Hz.

#### Preparation of the photocatalyst

**Preparation of  $g\text{-C}_3\text{N}_4$  nanosheets:**  $g\text{-C}_3\text{N}_4$  nanosheets were prepared by the reported sequential polymerization and liquid exfoliation routes with minor modification.<sup>74</sup> Typically, melamine (5 g) was calcined in a covered crucible (to prevent sublimation) at 550 °C with a heating rate of 5 °C min<sup>-1</sup> for 3 h in air atmosphere. After cooling down to room temperature, the resultant agglomerated yellow solid was milled into a powder. The as-synthesized bulk  $g\text{-C}_3\text{N}_4$  powder (0.1 g) was thoroughly dispersed in deionized water (100 mL) by sonication for 6 h. Hereafter, the resultant suspension was centrifuged at 5000 rpm to eliminate the remaining un-exfoliated  $g\text{-C}_3\text{N}_4$  for further use.

**Preparation of  $\gamma\text{-Fe}_2\text{O}_3$  NPs:**  $\gamma\text{-Fe}_2\text{O}_3$  NPs were synthesized by a reported chemical co-precipitation method using ferric and ferrous ions in alkali solution and with minor modifications.<sup>75</sup>  $\text{FeCl}_2\cdot 4\text{H}_2\text{O}$  (0.01 mol, 1.99 g) and  $\text{FeCl}_3\cdot 6\text{H}_2\text{O}$  (0.01 mol, 3.25 g) were dissolved in deionized water (30 mL) under argon atmosphere at room temperature. A solution of  $\text{NH}_4\text{OH}$  (0.6 M, 200 mL) was then added dropwise (drop rate = 1 mL·min<sup>-1</sup>) into the stirring mixture at ambient temperature. When the reaction pH reached 11, the addition of the  $\text{NH}_4\text{OH}$  solution was stopped. The obtained black dispersion was vigorously stirred for 1 h at room temperature. Then, the suspension was refluxing for 1 h to yield a brown dispersion. The resultant NPs were next separated by a magnetic bar, washed with deionized water (4 × 20 mL) and then dried overnight. Afterward, the obtained sample was heated at 200 °C with a heating rate of 2 °C min<sup>-1</sup> for 3 h to give the desired reddish-brown  $\gamma\text{-Fe}_2\text{O}_3$  NPs.

**Preparation of  $g\text{-C}_3\text{N}_4/\gamma\text{-Fe}_2\text{O}_3/\text{TiO}_2$ :** The magnetic  $g\text{-C}_3\text{N}_4/\gamma\text{-Fe}_2\text{O}_3/\text{TiO}_2$  was prepared by a reported sol-gel technique with minor modification.<sup>64</sup> In detail,  $g\text{-C}_3\text{N}_4$  nanosheets (1.5 g) and  $\gamma\text{-Fe}_2\text{O}_3$  NPs (0.67 g) were mixed with a solution of TBOT (5 mL), glacial acetic acid (G.A.A., 2 mL) and EtOH (10 mL) through the sonication for 1 h. Then, the suspension was stirred for 30 min at ambient temperature, followed by the dropwise addition of a solution of  $\text{H}_2\text{O}$ : EtOH (1:2, 7.5 mL) to produce a colloidal solution. The resultant colloidal solution was continuously stirred until the formation of  $\text{TiO}_2$  gel (~30 min). The obtained  $\text{TiO}_2$  gel was aged for 4 h at ambient temperature. After drying the as-prepared gel at 80 °C in an oven for 24 h, the xerogels were achieved. Finally, the magnetic  $g\text{-C}_3\text{N}_4/\gamma\text{-Fe}_2\text{O}_3/\text{TiO}_2$  was obtained through the calcination of the attained xerogels at 400 °C for 3 h, under an air atmosphere.

**Preparation of  $g\text{-C}_3\text{N}_4/\gamma\text{-Fe}_2\text{O}_3/\text{TiO}_2/\text{Pd}$ <sup>76</sup>:** The as-synthesized  $g\text{-C}_3\text{N}_4/\gamma\text{-Fe}_2\text{O}_3/\text{TiO}_2$  (0.5 g) was dispersed in deionized water (20 mL) by sonication for 30 min. Then, an aqueous solution of  $\text{Pd}(\text{OAc})_2$  (25 mL, 2M) was added dropwise to the dispersed suspension and continuous stirring was conducted 2 h. To this mixture, an aqueous solution of  $\text{NaBH}_4$  (30 mL, 0.1 M) was added portion by portion under vigorous stirring. After 4 h, the resultant  $g\text{-C}_3\text{N}_4/\gamma\text{-Fe}_2\text{O}_3/\text{TiO}_2/\text{Pd}$  was separated using an external magnet and washed repeatedly with

distilled water and ethanol (3 × 15 mL) before being dried under vacuum at 50 °C.

DOI: 10.1039/D0NJ01599G

#### General procedure for the photocatalytic fluoride-free Hiyama and Suzuki–Miyaura cross-coupling reactions under visible light irradiation

A 10-mL Pyrex test tube was charged with aryl halide (1 mmol), phenylboronic acid/triethoxyphenylsilane (1 mmol), NaOH (0.5 mmol), EtOH (4 mL) and  $g\text{-C}_3\text{N}_4/\gamma\text{-Fe}_2\text{O}_3/\text{TiO}_2/\text{Pd}$  (0.07 mol%). The reaction vessel was sealed with a rubber septum cap and transferred into a reactor chamber. To avoid the photothermal effect, first, the reaction vessel was submerged in a water bath at 25 °C and next irradiated at a distance of 10 cm with a white LED lamp (12 W). Meanwhile, the reaction mixture was magnetically stirred for an appropriate time (see Tables 2 and 3) at ambient temperature, under an air atmosphere. After the completion of the reaction, which was monitored by TLC, the mixture was allowed to be cooled to room temperature. Thereupon, the photocatalyst was easily separated by using a proper magnetic field, washed with EtOH (3 × 5 mL) and vacuum-dried at 50 °C to be ready for use in the next run. After the vacuum evaporation of the solvent, the crude product was subjected to a silica gel column chromatography (eluted with *n*-hexane: ethyl acetate; 50: 1) to afford the corresponding pure product.

#### Conclusions

In this work, a novel magnetically separable nanocomposite denoted as  $g\text{-C}_3\text{N}_4/\gamma\text{-Fe}_2\text{O}_3/\text{TiO}_2/\text{Pd}$  was successfully fabricated as an efficient visible-light harvesting photocatalyst. To characterize the as-synthesized photocatalyst, a variety of techniques including FT-IR, XPS, XRD, TEM, SEM, elemental mapping, VSM, DRS, and ICP analysis have been employed. Interestingly,  $g\text{-C}_3\text{N}_4/\gamma\text{-Fe}_2\text{O}_3/\text{TiO}_2/\text{Pd}$  was found to be an excellent photocatalyst to promote the fluoride-free Hiyama and Suzuki–Miyaura cross-coupling reactions of a broad range of aryl iodides/bromides and most importantly the highly challenging aryl chloride, which are far extensively available and cheaper than aryl iodides/bromides, with triethoxyphenylsilane/phenylboronic acid, at room temperature under visible light irradiation. The superior photocatalytic activity of  $g\text{-C}_3\text{N}_4/\gamma\text{-Fe}_2\text{O}_3/\text{TiO}_2/\text{Pd}$  could be attributed to the synergistic catalytic effects of Pd NPs and  $g\text{-C}_3\text{N}_4/\gamma\text{-Fe}_2\text{O}_3/\text{TiO}_2$ . The presented photocatalytic system can be magnetically separated and conveniently recycled at least seven times without a discernible decrease in its activity. Furthermore, the filtration test and poisoning experiments efficiently confirmed that the as-synthesized nanocatalyst is heterogeneous and completely stable under the reaction conditions. Moreover, the cross-coupling reaction showed the capability of being scaled-up, which is a significant aspect of the industrial and pharmaceutical applications of the resulting biaryls. Utilizing the sustainable and safe light source, no need to use any additive or heat, and using an eco-friendly solvent are other advantages that support the current protocol towards the green chemistry. The use of the presented new photocatalyst to promote the alternative cross-coupling reactions is ongoing in our laboratory.

## Conflicts of interest

There are no conflicts to declare.

## Acknowledgments

Financial support of this project by the University of Birjand Research Council and the XPS facilities of the University of Alicante is appreciated.

## References

- C. J. Li and B. M. Trost, *Proc. Natl. Acad. Sci.*, 2008, **105**, 13197-13202.
- N. S. Lewis and D. G. Nocera, *Proc. Natl. Acad. Sci.*, 2006, **103**, 15729-15735.
- D. M. Schultz and T. P. Yoon, *Science*, 2014, **343**, 1239176.
- B. Roose, S. Pathak and U. Steiner, *Chem. Soc. Rev.*, 2015, **44**, 8326-8349.
- Z. Zhao, Y. Long, S. Luo, W. Wu and J. Ma, *New J. Chem.*, 2019, **43**, 6294-6302.
- A. O. Ibhadon and P. Fitzpatrick, *Catalysts*, 2013, **3**, 189-218.
- R. Daghrir, P. Drogui and D. Robert, *Ind. Eng. Chem. Res.*, 2013, **52**, 3581-3599.
- X. Kang, S. Liu, Z. Dai, Y. He, X. Song and Z. Tan, *Catalysts*, 2019, **9**, 191.
- Z. Zeng, K. Li, K. Wei, Y. Dai, L. Yan, H. Guo and X. Luo, *Chin. J. Catal.*, 2017, **38**, 498-507.
- Z. Li, F. Raziq, C. Liu, L. Bai and L. Jing, *Curr. Opin. Green Sustain. Chem.*, 2017, **6**, 57-62.
- S. Patnaik, S. Martha, S. Acharya and K. M. Parida, *Inorg. Chem. Front.*, 2016, **3**, 336-347.
- Z. Tong, D. Yang, Z. Li, Y. Nan, F. Ding, Y. Shen and Z. Jiang, *ACS nano*, 2017, **11**, 1103-1112.
- J. Li, Y. Liu, H. Li and C. Chen, *J. Photochem. Photobiol. A Chem.*, 2016, **317**, 151-160.
- A. J. Lennox and G. C. Lloyd-Jones, *Chem. Soc. Rev.*, 2014, **43**, 412-443.
- A. Monfared, R. Mohammadi, S. Ahmadi, M. Nikpassand and A. Hosseini, *RSC Adv.*, 2019, **9**, 3185-3202.
- C. C. Johansson Seechurn, M. O. Kitching, T. J. Colacot and V. Snieckus, *Angew. Chem. Int. Ed.*, 2012, **51**, 5062-5085.
- Y. Nakao and T. Hiyama, *Chem. Soc. Rev.*, 2011, **40**, 4893-4901.
- T. Hiyama and Y. Hatanaka, *Pure Appl. Chem.*, 1994, **66**, 1471-1478.
- Y. Hatanaka and T. Hiyama, *Synlett*, 1991, **1991**, 845-853.
- J. H. Li, C. L. Deng, W. J. Liu and Y. X. Xie, *Synthesis*, 2005, **2005**, 3039-3044.
- B. C. Ranu, R. Dey and K. Chattopadhyay, *Tetrahedron Lett.*, 2008, **49**, 3430-3432.
- S. Sobhani, A. Habibollahi and Z. Zeraatkar, *Org. Process Res. Dev.*, 2019, **23**, 1321-1332.
- N. Kambe, T. Iwasaki and J. Terao, *Chem. Soc. Rev.*, 2011, **40**, 4937-4947. DOI: 10.1039/D0NJ01599G
- M. Pagliaro, V. Pandarus, R. Ciriminna, F. Béland and P. Demma Carà, *ChemCatChem*, 2012, **4**, 432-445.
- D. Astruc, F. Lu and J. R. Aranzas, *Angew. Chem. Int. Ed.*, 2005, **44**, 7852-7872.
- G. M. Scheuermann, L. Rumi, P. Steurer, W. Bannwarth and R. Mülhaupt, *J. Am. Chem. Soc.*, 2009, **131**, 8262-8270.
- B. Karimi, D. Elhamifar, J. H. Clark and A. J. Hunt, *Chem.: Eur. J.*, 2010, **16**, 8047-8053.
- S. Schweizer, J. M. Becht and C. Le Drian, *Tetrahedron*, 2010, **66**, 765-772.
- A. Grirrane, H. Garcia and A. Corma, *J. Catal.*, 2013, **302**, 49-57.
- B. H. Nguyen, A. Redden and K. D. Moeller, *Green Chem.*, 2014, **16**, 69-72.
- M. Hosseini-Sarvari and Z. Bazyar, *ChemistrySelect*, 2018, **3**, 1898-1907.
- Q. Xiao, S. Sarina, A. Bo, J. Jia, H. Liu, D. P. Arnold, Y. Huang, H. Wu and H. Zhu, *ACS Catal.*, 2014, **4**, 1725-1734.
- F. Feizpour, M. Jafarpour and A. Rezaeifard, *Catal. Lett.*, 2019, **149**, 1595-1610.
- K. Mori, M. Kawashima and H. Yamashita, *Chem. Commun.*, 2014, **50**, 14501-14503.
- F. Wang, C. Li, H. Chen, R. Jiang, L. D. Sun, Q. Li, J. Wang, J. C. Yu and C. H. Yan, *J. Am. Chem. Soc.*, 2013, **135**, 5588-5601.
- Q. Xiao, S. Sarina, E. Jaatinen, J. Jia, D. P. Arnold, H. Liu and H. Zhu, *Green Chem.*, 2014, **16**, 4272-4285.
- M. Koohgard and M. Hosseini-Sarvari, *Catal. Commun.*, 2018, **111**, 10-15.
- S. Rohani, A. Ziarati, G. M. Ziarani, A. Badiei and T. Burgi, *Catal. Sci. Technol.*, 2019, **9**, 3820-3827.
- S. Zhang, C. Chang, Z. Huang, Y. Ma, W. Gao, J. Li and Y. Qu, *ACS Catal.*, 2015, **5**, 6481-6488.
- Z. J. Wang, S. Ghasimi, K. Landfester and K. A. Zhang, *Chem. Mater.*, 2015, **27**, 1921-1924.
- Z. Jiao, Z. Zhai, X. Guo and X. Y. Guo, *J. Phys. Chem. C*, 2015, **119**, 3238-3243.
- S. Gao, N. Shang, C. Feng, C. Wang and Z. Wang, *RSC Adv.*, 2014, **4**, 39242-39247.
- A. Xie, K. Zhang, F. Wu, N. Wang, Y. Wang and M. Wang, *Catal. Sci. Technol.*, 2016, **6**, 1764-1771.
- D. Han, Z. Bao, H. Xing, Y. Yang, Q. Ren and Z. Zhang, *Nanoscale*, 2017, **9**, 6026-6032.
- Y. Li, Z. Zhang, L. Pei, X. Li, T. Fan, J. Ji, J. Shen and M. Ye, *Appl. Catal. B Environ.*, 2016, **190**, 1-11.
- X. H. Li, M. Baar, S. Blechert and M. Antonietti, *Sci. Rep.*, 2013, **3**, 1743.
- S. Sobhani, H. Hosseini Moghadam, J. Skibsted and J. M. Sansano, *Green Chem.*, 2020, **22**, 1353-1365.
- S. Sobhani, Z. Mesbah Falatoni, S. Asadi and M. Honarmand, *Catal. Lett.*, 2016, **146**, 255-268.

## Journal Name

## ARTICLE

- 1  
2  
3  
4  
5  
6  
7  
8  
9  
10  
11  
12  
13  
14  
15  
16  
17  
18  
19  
20  
21  
22  
23  
24  
25  
26  
27  
28  
29  
30  
31  
32  
33  
34  
35  
36  
37  
38  
39  
40  
41  
42  
43  
44  
45  
46  
47  
48  
49  
50  
51  
52  
53  
54  
55  
56  
57  
58  
59  
60
- 49 S. Sobhani, Z. Vahidi, Z. Zeraatkar and S. Khodadadi, *RSC Adv.*, 2015, **5**, 36552-36559.
- 50 A. Thomas, A. Fischer, F. Goettmann, M. Antonietti, J. O. Müller, R. Schlögl and J. M. Carlsson, *J. Mater. Chem.*, 2008, **18**, 4893-4908.
- 51 V. N. Khabashesku, J. L. Zimmerman and J. L. Margrave, *Chem. Mater.*, 2000, **12**, 3264-3270.
- 52 Z. Yang, J. Yan, J. Lian, H. Xu, X. She and H. Li, *ChemistrySelect*, 2016, **1**, 5679-5685.
- 53 Y. Gao, Y. Masuda, Z. Peng, T. Yonezawa and K. Koumoto, *J. Mater. Chem.*, 2003, **13**, 608-613.
- 54 A. Habibi-Yangjeh, M. Mousavi and K. Nakata, *J. Photochem. Photobiol. A Chem.*, 2019, **368**, 120-136.
- 55 Z. Tong, D. Yang, T. Xiao, Y. Tian and Z. Jiang, *Chem. Eng. J.*, 2015, **260**, 117-125.
- 56 X. Liu, A. Jin, Y. Jia, J. Jiang, N. Hu and X. Chen, *RSC Adv.*, 2015, **5**, 92033-92041.
- 57 A. Mirzaei, Z. Chen, F. Haghghat and L. Yerushalmi, *Appl. Catal. B Environ.*, 2019, **242**, 337-348.
- 58 M. H. Pham, C. T. Dinh, G. T. Vuong, N. D. Ta and T. O. Do, *Phys. Chem. Chem. Phys.*, 2014, **16**, 5937-5941.
- 59 B. J. Tan, K. J. Klabunde and P. M. Sherwood, *Chem. Mater.*, 1990, **2**, 186-191.
- 60 R. Suresh, K. Giribabu, R. Manigandan, A. Stephen and V. Narayanan, *RSC Adv.*, 2014, **4**, 17146-17155.
- 61 M. Blanco, D. Mosconi, C. Tubaro, A. Biffis, D. Badocco, P. Pastore, M. Otyepka, A. Bakandritsos, Z. Liu, W. Ren and S. Agnoli, *Green Chem.*, 2019, **21**, 5238-5247.
- 62 F. Raza, D. Yim, J. H. Park, H. I. Kim, S. J. Jeon and J. H. Kim, *J. Am. Chem. Soc.*, 2017, **139**, 14767-14774.
- 63 L. Zhong, A. Chokkalingam, W. S. Cha, K. S. Lakhi, X. Su, G. Lawrence and A. Vinu, *Catal. Today*, 2015, **243**, 195-198.
- 64 X. N. Wei and H. L. Wang, *J. Alloys Compd.*, 2018, **763**, 844-853.
- 65 G. Salazar-Alvarez, J. Sort, A. Uheida, M. Muhammed, S. Surinach, M. D. Baró and J. Nogués, *J. Mater. Chem.*, 2007, **17**, 322-328.
- 66 D. Cao, H. Li, L. Pan, J. Li, X. Wang, P. Jing, X. Cheng, W. Wang, J. Wang and Q. Liu, *Sci. Rep.*, 2016, **6**, 1-9.
- 67 D. A. Horton, G. T. Bourne and M. L. Smythe, *Chem. Rev.*, 2003, **103**, 893-930.
- 68 F. X. Felpin and S. Sengupta, *Chem. Soc. Rev.*, 2019, **48**, 1150-1193.
- 69 J. A. García-López and M. F. Greaney, *Chem. Soc. Rev.*, 2016, **45**, 6766-6798.
- 70 C. Deraedt and D. Astruc, *Acc. Chem. Res.*, 2014, **47**, 494-503.
- 71 S. Sarina, H. Zhu, E. Jaatinen, Q. Xiao, H. Liu, J. Jia, C. Chen and J. Zhao, *J. Am. Chem. Soc.*, 2013, **135**, 5793-5801.
- 72 K. Sharma, M. Kumar and V. Bhalla, *Chem. Commun.*, 2015, **51**, 12529-12532.
- 73 H. H. Shin, E. Kang, H. Park, T. Han, C. H. Lee and D. K. Lim, *J. Mater. Chem. A*, 2017, **5**, 24965-24971.
- 74 X. Zhang, X. Xie, H. Wang, J. Zhang, B. Pan and Y. Xie, *J. Am. Chem. Soc.*, 2013, **135**, 18-21. DOI: 10.1039/D0NJ01599G
- 75 S. Sobhani and R. Jahanshahi, *New J. Chem.*, 2013, **37**, 1009-1015.
- 76 M. Ma, Q. Zhang, D. Yin, J. Dou, H. Zhang and H. Xu, *Catal. Commun.*, 2012, **17**, 168-172.



**g-C<sub>3</sub>N<sub>4</sub>/γ-Fe<sub>2</sub>O<sub>3</sub>/TiO<sub>2</sub>/Pd: A new magnetically separable photocatalyst for visible-light-driven fluoride-free Hiyama and Suzuki–Miyaura cross-coupling reactions at room temperature**

Roya Jahanshahi, Asma Khazaei, Sara Sobhani\* and José Miguel Sansano

g-C<sub>3</sub>N<sub>4</sub>/γ-Fe<sub>2</sub>O<sub>3</sub>/TiO<sub>2</sub>/Pd is developed as a new magnetically separable photocatalyst for the efficient fluoride-free Hiyama and Suzuki–Miyaura cross-coupling reactions at room temperature under visible light irradiation.

